Ab Initio Calculations on the (1)$^2\Delta$ Excited State and Low-Lying Quartet States of Ga•N_2: Simulation of Its LIF Spectrum

Edmond P. F. Lee,[†] John M. Dyke,*[,†] Daniel K. W. Mok,[‡] Robert P. Claridge,[§] and Foo-Tim Chau[‡]

Department of Chemistry, Southampton University, Highfield, Southampton SO17 1BJ, England, U.K., Department of Applied Biology and Chemical Technology, Hong Kong Polytechnic University, Hung Hom, Kowloon, Hong Kong, and DERA, Fort Halstead, Sevenoaks, Kent, U.K.

Received: May 21, 2001; In Final Form: July 12, 2001

The $^2\Delta$ and $^4\Sigma^-$ excited states of Ga•N_2, which were assigned by Ellis et al. (*Phys. Chem. Chem. Phys*. **1999**, *1*, 2709) to the upper states of two LIF transitions observed from the Ga•N_2 $\tilde{X}^2\Pi$ state with onsets of 33 468 and 37 633 cm^{-1}, respectively, have been studied by high-level ab initio calculations. Minimum-energy geometrical parameters, harmonic vibrational frequencies, and relative energies were computed at the SERHF, CASSCF, B3LYP, MP2, QCISD, and CCSD(T) levels of calculation, using standard and specifically designed, all-electron and ECP (for Ga) basis sets of up to aug-cc-pVQZ quality. In addition, the low-lying linear $^4\Pi$ and a number of T-shaped quartet states of Ga•N_2 were also studied. Franck−Condon factors (FCFs) of selected electronic transitions were calculated. Absorption spectra were simulated by employing the computed FCFs. On the basis of ab initio results and spectral simulations, the assignment of the 33 468 cm^{-1} LIF band is concluded to be the $^2\Delta_{3/2} \leftarrow {}^2\Pi_{1/2}$ transition of Ga•N_2. In addition, the measured T_0 position of this band is confirmed and the assignments of the observed vibrational progressions in this LIF band have been revised. As for the 37 633 cm^{-1} LIF band, ab initio results and spectral simulations computed in this work do not support the assignment of the upper state as the $^4\Sigma^-$ state of Ga•N_2, which was shown by ab initio calculations to be a charge-transfer state with a short computed Ga−N bond length (ca. 2.0 Å) and large intermolecular vibrational frequencies (>200 cm^{-1}). In addition, all low-lying Ga•N_2 quartet states considered were found to be either very weakly bound van der Waals states (Ga−N bond length ca. 5 Å) or well-bound charge transfer states, and none of them can be assigned to the upper state of this LIF band. Doubts concerning the identity of the molecular carrier and the electronic states involved in this LIF band remain. Finally, the stabilities of the charge-transfer quartet states of Ga•N_2 investigated in this work have been rationalized in terms of bonding interaction between the HOMOs of Ga and the LUMOs of N_2 and electrostatic attraction resulting from charge transfer from Ga to N_2. Possible applications of this kind of bonding and charge-transfer interactions in an M•N_4 ring system have been discussed briefly in relation to stabilizing an N_n system, where M•N_n represents a potential high energy density material.

Introduction

Recently, we have reported a high-level ab initio study on the lowest-lying $^2\Pi$, $^2\Sigma$, $^2A_1$, $^2B_1$, and $^2B_2$ states of the Ga•N_2 complex.[1] In this study, the ground state of Ga•N_2 was established to be the $\tilde{X}^2\Pi$ state and the interaction energy of complex formation, ΔE_e(CP)(Ga•N_2 $\tilde{X}^2\Pi$), which included allowance for the full counterpoise (CP) correction[2] for basis set superposition error (BSSE), core correlation, and a relativistic correction, was calculated to be −1.1 kcal•mol^{-1} (−400 cm^{-1}) at the RCCSD(T) level with basis sets of better than augmented−polarized−valence−quadruple-ζ (aug-cc-pVQZ) quality. Including spin−orbit interaction, the best estimates of D_0 and enthalpy of formation at 298 K for the $\tilde{X}^2\Pi_{1/2,3/2}$ spin−orbit states were evaluated to be $D_0 = 95, 320$ cm^{-1} and $\Delta H^{298K} = 0.07, -0.58$ kcal mol^{-1}, respectively. One of the aims of this study (ref 1) was to lay the foundation for further investigation on low-lying excited states of Ga•N_2, with a view to establishing the assignments of two observed LIF bands (with onsets at 33 468 and 37 633 cm^{-1}) reported and tentatively assigned by Ellis et al.[3] to the $^2\Delta \leftarrow \tilde{X}^2\Pi_{3/2}$ and $^4\Sigma^- \leftarrow \tilde{X}^2\Pi$ transitions, respectively, of Ga•N_2. These suggested assignments were made by comparing the observed Ga•N_2 band systems with nearby atomic gallium transitions, as these transitions were expected to correspond to transitions between the dissociation limits of the states involved in Ga•N_2, and noting the long excited-state fluorescence lifetime (ca. 2 μs) of the upper state for the band with an onset of 37 633 cm^{-1}. In the present study, we report ab initio calculations on the $^2\Delta$, $^4\Sigma^-$ and also some other low-lying quartet states of Ga•N_2 for the first time. Franck−Condon factor (FCF) calculations on selected electronic absorptions have also been carried out, employing the ab initio force constants and geometries of the electronic states involved, obtained in this work. With the aid of high-level ab initio calculations and spectral simulations based on the computed FCFs, it is hoped that the assignments of the two LIF bands observed by Ellis et al.[3] could be established.

In the search for a suitable candidate for the upper state of the LIF band at 37 633 cm^{-1} (see later text), a number of low-lying linear and T-shaped quartet states of Ga•N_2 were investigated for the first time. Some of these states were found to be well-bound charge-transfer states. The interaction between a p-block metal center and a dinitrogen molecule in these states has been understood in terms of bonding combinations between the metal HOMOs and dinitrogen LUMOs and electrostatic attraction resulting from charge transfer from the metal center

[†] Southampton University.
[‡] Hong Kong Polytechnic University.
[§] DERA.

10.1021/jp011925j CCC: $20.00
Published on Web 09/15/2001

to the dinitrogen molecule. Possible applications of this kind of metal−dinitrogen interaction in the stabilization of polynitrogen species, which have been considered as possible candidates of high-energy-density materials (HEDM),[4] are briefly discussed.

Computational Details

Ab Initio Calculations. Initial investigation was focused on the $^2\Delta$ and $^4\Sigma^-$ states of Ga•N_2, which were tentatively assigned to the upper states of the two observed LIF bands by Ellis et al.[3] For the $^4\Sigma^-$ state, with the $...\sigma^1\pi^2$ open-shell electronic configuration, geometry optimization and harmonic vibrational frequency calculations were carried out at the CASSCF(3,6), UB3LYP, UMP2, UQCISD, and UCCSD(T) levels. Various standard basis sets and an effective-core-potential (ECP) basis set, lanl2[8s6p5d2f], which was designed for Ga [coupled with the 6-311+G(3df) basis set for N] and described in ref 1, were employed in these calculations. All the above calculations were performed using the Gaussian98 suite of programs.[5] In addition, symmetry-equivalent restricted-spin Hartree−Fock (SERHF) calculations were also carried out employing the GAMES-UK suite of programs.[6] In the SERHF calculations, the split-valence basis sets of Dunning and Hay[7] {[6s4p1d] for Ga and [3s2p] for N} were employed and augmented with uncontracted s (exponent: 0.020451), p (0.017514), sp (0.005), and d (0.03, 0.01, 0.003 333) functions on Ga and s (0.060 943), p (0.0472571), and d (1.654, 0.469) on N. The augmented d functions on Ga were designed to account adequately for the 4d atomic orbital of Ga, as shown from the wave function of an ROHF calculation on the $^2\Delta$ state of Ga•N_2 obtained using these basis sets (see later text).

For the $^2\Delta$ state of Ga•N_2, with the $...\sigma^2\delta^1$ open-shell electronic configuration, the singly occupied, doubly degenerate δ molecular orbitals originate essentially from the 4d atomic orbitals of Ga, which are unoccupied in the ground-state electronic configuration of atomic gallium ($...3d^{10}4s^24p^1$). Consequently, standard basis sets available in the literature, which were designed for neutral ground states of atomic elements, are inadequate for calculations on the $^2\Delta$ state of Ga•N_2. In this connection, the above-mentioned augmented split-valence basis sets were designed and used in the SERHF calculations on the $^2\Delta$ state. In addition, uncontracted diffuse sp (exponent: 0.002) and d (0.017 625, 0.004 406 25) functions were augmented to the 6-31+G(2d) basis set of Ga, while sp (0.002) and d (0.018 777, 0.006 259 25, 0.002 086 41) functions were added to the 6-311+G(3d) basis set of Ga, for the same purpose. The ROHF wave functions of the $^2\Delta$ state of Ga•N_2 obtained with these augmented basis sets show that the augmentations in the d orbital space are adequate for the singly occupied δ molecular orbitals.

In addition to the extra requirements considered above for the basis sets used in the calculations on the $^2\Delta$ state of Ga.N_2, it was found that all the unrestricted-spin Hartree−Fock (UHF) based calculations {UB3LYP, UMP2, UQCISD, and UCCSD(T)} on the $^2\Delta$ state collapsed to the $\tilde{X}^2\Pi$ state at the SCF stage. Nevertheless, restricted-spin methods, such as the SERHF, CASSCF(3,6), and RCCSD(T) (see next paragraph) methods, worked well for the $^2\Delta$ state. For CASSCF calculations, requesting the fifth root gives the $^2\Delta$ state. Geometry optimization and harmonic vibrational frequency calculations employing analytic first and second energy derivatives, respectively, were successful for the $^2\Delta$ state with the SERHF and CASSCF methods. The CASSCF force constants of the $^2\Delta$ state were employed in the subsequent multidimensional harmonic FCF calculations (to be discussed below) for transitions involving the $^2\Delta$ state. [The UCCSD(T)/6-311+G(3df) force constants from ref 1 were used for the $\tilde{X}^2\Pi$ state, unless otherwise stated; see also later text.]

Further geometry optimization calculations on the $\tilde{X}^2\Pi$ and $^2\Delta$ states of Ga•N_2 were carried out at the RCCSD(T) level,[8] employing the MOLPRO suite of programs,[9] with an ECP basis set, ECP[7s7p5d2f], for Ga and the aug-cc-pVTZ basis set for N. The ECP employed for Ga is the quasi-relativistic effective core potential (ECP28MWB) of Stuttgart.[9,10] The corresponding valence basis set consists of single sets of contracted s, p, and d functions complemented with uncontracted s, p, d, and f functions. The contracted s, p, and d functions consist of 15 s (highest exponent, 7.0; ratio, 2.0), 11 p (2.5; 2.0), and 7 d (0.54; 3.0) primitives. The contraction coefficients of the contracted s and p functions were obtained from an ROHF calculation on atomic gallium, employing the sets of s and p primitives uncontracted, while those for the d contraction were obtained from an ROHF calculation on the $^2\Delta$ state of Ga•N_2, employing the d primitives uncontracted. The uncontracted 6 s, 6 p, 4 d, and 2 f functions have the following exponents: s (highest exponents, 0.65; ratio, 3.0), p (0.9; 3.2), d (0.2; 4.0), and f (exponents of 0.1 and 0.02), respectively.

Relative electronic energies were calculated at higher levels of theory. Vertical excitation energies (VEEs) from the $\tilde{X}\ ^2\Pi$ state to the $^2\Delta$ and $^4\Sigma^-$ states of Ga•N_2 were computed at the CASSCF/MRCI/ECP[10s8p5d], aug-cc-pVTZ(no f), RCCSD(T)/ECP[11s10p6d5f], ug-cc-pVQZ(no g), and RCCSD(T)/ECP[11s10p6d5f3g], aug-cc-pVQZ levels (with the ECP and aug-cc-pVXZ basis sets for Ga and N, respectively), employing MOLPRO.[9] The ECP[11s10p6d5f3g] basis set of Ga has been described previously,[1] and the ECP[11s10p6d5f] basis set has 3 g functions removed from the ECP[11s10p6d5f3g] basis set. The ECP[10s8p5d] basis set used for the CASSCF/MRCI calculations has the same s and p contracted functions as the ECP[11s10p6d5f3g] basis set described previously.[1] The uncontracted 9 s, 7 p, and 5 d functions have the following exponents: s (highest exponent, 0.65; ratio, 2.75), p (0.9; 3.0), and d (0.25; 3.0). The CASSCF calculations on the $\tilde{X}^2\Pi$ and $^4\Sigma^-$ states considered 13 valence electrons within an active space of seven σ and three sets of π (b_1 and b_2 symmetry in the C_{2v} point group) molecular orbitals. For the $^2\Delta$ state, an active space of seven σ, two sets of π, and two δ (a_2 symmetry in the C_{2v} point group) molecular orbitals was employed. The internally contracted MRCI calculation[11] on each state has employed the CASSCF orbitals of the corresponding state as the many-particle basis. The numbers of uncontracted and internally contracted configurations in the MRCI calculation for each state are larger than 430 and 4.1 millions, respectively. For the $^2\Delta$ state, the CP-corrected[2] interaction energy, ΔE_e(CP) (or D_e), for complex formation was computed at the RCCSD(T)/ECP[11s10p6d5f3g], aug-cc-pVQZ//RCCSD(T)/ECP[7s7p5d2f], aug-cc-pVTZ level.

In addition to the $\tilde{X}^2\Pi$, $^2\Delta$, and $^4\Sigma^-$ states, a number of low-lying quartet states of linear and T-shaped structures have also been studied. The methods and basis sets employed in these calculations are similar to those described above and will not be repeated. The details of these calculations will be presented when their results are discussed in the Result and Discussion.

Franck−Condon Factor Calculations and Spectral Simulations. Multidimensional harmonic Franck−Condon factor (FCF) calculations were carried out on a number of selected absorption transitions to aid spectral assignment. The method employed, which is within the harmonic oscillator model and includes Duschinsky rotation, has been described previously.[12,13]

TABLE 1: Optimized Geometry (Å) and Harmonic Vibrational Frequencies (cm^{-1}) of the ...$\sigma^2\delta^1$ $^2\Delta$ State of Ga•N_2 at Different Levels of Calculations

method	GaN	NN	ω_1(NN)	$\omega_2(\sigma)$	$\omega_3(\pi)$
SERHF/SV+diff+polarization[a]	3.1574	1.0771	2730.1	71.3	104.7
CASSCF(3,6,root=5)/6-31+G(2d)+diff[b]	3.1669	1.1071	2752.2	64.3	120.7
CASSCF(3,6,root=5)/6-311+G(3d)+diff[c]	3.2464	1.0668	2727.3	62.1	81.2
RCCSD(T)/ECP[7s7p5d2f];aug-cc-pVTZ[d]	2.9626	1.1032		85.0[e]	

[a] See text for the details of the basis sets used; the optimized geometry for the $\tilde{X}^2\Pi$ state at this level of calculation is r(GaN) = 3.5329 and r(NN) = 1.0777 Å. [b] See text for the details of the basis sets used; the optimized geometry for the $\tilde{X}^2\Pi$ state at this level of calculation is r(GaN) = 3.9015 and r(NN) = 1.0718 Å. [c] See text for the details of the basis sets used; the optimized geometry for the $\tilde{X}^2\Pi$ state at this level of calculation is r(GaN) = 4.0090 and r(NN) = 1.0608 Å. [d] See text for the details of the basis sets used; the optimized geometry for the $\tilde{X}^2\Pi$ state at this level of calculation is r(GaN) = 3.3229 and r(NN) = 1.1039 Å. [e] From one-dimensional energy scan; the corresponding value for the $\tilde{X}^2\Pi$ state is 47.0 cm^{-1}.

In addition, one-dimensional energy scans of the $\tilde{X}^2\Pi$ and $^2\Delta$ states of Ga•N_2 in the GaN coordinate (R; NN fixed to 1.1036 Å, the average of the optimized NN bond lengths obtained for the two states; see next section) were carried out at the RCCSD-(T)/ECP[7s7p5d2f], aug-cc-pVTZ level. The one-dimensional curves thus obtained were then employed to compute vibrational wave functions of the Ga−N_2 stretching mode of the two states considered. On the basis of a pseudodiatomic approximation, which treats N_2 as a single entity, the radial Schrödinger equation was solved using the program, LEVEL,[14] where the Ga−N_2 potential was obtained by interpolating 26 RCCSD(T) single-point energies for each state using cubic spline functions and by extrapolation to the dissociation limit. The extrapolated values were obtained from the relationship

$$V = D_e - C_5/R^5 + C_6/R^6$$

where the coefficients C_5 and C_6 were determined by least-squares fitting of a few RCCSD(T) single-point energies at large R. The RCCSD(T) dissociation energies, D_e, of the $^2\Delta$ and $^2\Pi$ states used in the extrapolation have been calculated in this work (this is mentioned earlier; also see next section) and ref 1, respectively. On the basis of the parallel mode approximation (see ref 12 and references therein), the FCFs in the Ga−N_2 stretching mode of the absorption from the $\tilde{X}^2\Pi$ state to the $^2\Delta$ state were calculated by numerical integration also using LEVEL.[14]

Computed FCFs were used to simulate the observed LIF spectrum, employing a Gaussian peak shape with a full-width at half-maximum (fwhm) of 10 cm^{-1} for each vibrational component. It should be noted that the simulated spectrum obtained based on the computed pseudodiatomic one-dimensional FCFs has two advantages over that based on the multidimensional harmonic FCFs. First, the force constants of the $^2\Delta$ state used in the multidimensional harmonic FCF calculations were obtained at the CASSCF level, a method which lacks dynamic electron correlation. The RCCSD(T) level of calculation, used to obtain the potential energy curve for the $\tilde{X}^2\Pi$ and $^2\Delta$ states for the pseudodiatomic one-dimensional FCF calculations, is of a considerably higher level than the CASSCF level used to obtain the force constants for the multidimensional FCF calculations. It will be shown later in the comparison between the computed and observed vibrational frequencies that there is a closer agreement between the computed Ga−N_2 stretching frequency of the $^2\Delta$ state obtained from the RCCSD-(T) one-dimensional pseudodiatomic surface and the observed vibrational intervals in the LIF band than those obtained from the CASSCF calculations. Second, the computed pseudodiatomic one-dimensional FCFs include anharmonicities via the numerical solution of the Schrodinger equation using the RCCSD(T) curves. However, a simulated spectrum obtained based on the computed multidimensional harmonic FCFs also has advantages over that based on the pseudodiatomic one-dimensional FCFs, as the former includes the Duschinsky effect and considers all vibrational modes.

Results and Discussion

$^2\Delta$ State and LIF Band at 33 468 cm^{-1}. The ab initio results obtained from this work are summarized in Tables 1−9. The $^2\Delta$ state and the LIF band observed with an onset at 33 468 cm^{-1}, which was assigned to the $^2\Delta \leftarrow \tilde{X}^2\prod$ absorption of Ga•N_2 by Ellis et al.,[3] are considered first. From Table 1, the computed bond lengths and harmonic vibrational frequencies of the $^2\Delta$ state suggest a weakly bound complex with a long GaN distance and low intermolecular vibrational frequencies. Nevertheless, the computed GaN bond lengths of the $^2\Delta$ state are consistently shorter than those of the $\tilde{X}^2\Pi$ state (for the same levels of calculation; see footnotes of Table 1), suggesting that the former state is relatively more strongly bound than the latter state. This is as expected, on the basis of qualitative considerations of electron−electron repulsion and the orientation of the singly occupied molecular orbitals, which have been discussed briefly in ref 3 (see also references therein). Regarding the computed vibrational frequencies, the intermolecular Ga−N_2 stretching values obtained at different levels of calculation have a spread of 23 cm^{-1}. The consistency in the computed Ga−N stretching frequencies suggests that these calculated values are reasonably reliable, although these computed van der Waals stretching frequencies are quite small. In a comparison of the computed Ga−N_2 stretching frequencies with the observed value assigned to the Ga−N_2 stretching mode by Ellis et al.,[3] the computed CASSCF harmonic frequencies are smaller than the ω_e value of 94.4 cm^{-1} derived from the measured vibrational intervals of the main progression of the LIF band at 33 468 cm^{-1} by ca. 30 cm^{-1}. Nevertheless, the RCCSD(T) value of 85.0 cm^{-1} obtained from the one-dimensional energy scan is in very good agreement with the experimentally derived ω_e value. It is concluded that the computed vibrational frequencies obtained here support the assignment made by Ellis et al.[3] on the observed main vibrational progression to the van der Waals stretching mode of the $^2\Delta$ state of Ga•N_2.

Considering computed relative energies, the computed vertical excitation energies (VEEs) from the $\tilde{X}^2\Pi$ state to the $^2\Delta$ state obtained at different levels of calculation are given in Table 2 and compared with the estimated position of the vibrational component with maximum observed intensity (the fifth peak of the main series; see Figure 1c and later text). The computed VEE values obtained at different levels of calculation are consistent to within ca. 0.1 eV, suggesting that these values should be reasonably reliable. When these computed values are compared with the observed value, they are smaller by ca. 0.2 eV. The T_e value has also been calculated at the RCCSD(T)/

TABLE 2: Computed Vertical Excitation Energies (VEEs) of the $...\sigma^2\delta^1\ ^2\Delta$, $...\sigma^1\pi^2\ ^4\Sigma^-$, and $...\sigma^1\pi^1\sigma^1\ ^4\Pi$ States of Ga•N_2 from the $...\sigma^2\pi^1\ \tilde{X}^2\Pi$ State[a]

		$^2\Delta$		$^4\Sigma^-$		$^4\Pi$	
method	basis set Ga/N	eV	cm^{-1}	eV	cm^{-1}	eV	cm^{-1}
MRCI[b]	ECP-[10s8p5d]/aug-cc- pVTZ(no f)	3.832	30 904	3.237	26 107		
MRCI+D[b]	as above	3.978	32 082	3.940	31 782		
RCCSD	as above	3.988	32 162	4.214	33 988		
RCCSD(T)	as above	3.997	32 236	4.238	34 185		
RCCSD	ECP-[11s10p6d5f]/aug- cc-pVQZ(no g)	3.930	31 697	4.189	33 788	4.377	35 302
RCCSD(T)	as above	3.937	31 751	4.215	33 997	4.402	35 501
RCCSD	ECP-[11s10p6d5f3g]/aug-cc-pVQZ	3.930	31 697	4.390	35 411		
RCCSD(T)	as above	3.936	31 748	4.217	34 016		
RCCSD[c]	as above	3.913	31 559	4.160	33 553	4.437	35 789
RCCSD(T)[c]	as above	3.919	31 611	4.187	33 773	4.463	35 999
exptl[d]		4.192	33 814	4.727	38 123		

[a] At the QCISD/lanl2-[8s7p4d]/6-311+G(3d) optimized geometry (GaN = 3.4864 and NN = 1.0999 Å) of the $\tilde{X}^2\Pi$ state of Ga•N_2, except otherwise stated (from ref 1; see footnote *c*). [b] See text for the details of the basis sets and the active space used in the CASSCF and MRCI calculations. [c] At the UCCSD(T)/6-311+G(3df) geometry of the $\tilde{X}^2\Pi$ state of Ga•N_2 (GaN = 3.2905 and NN = 1.0973 Å; from ref 1). [d] Ellis et al.;[3] estimated positions of the vibrational components with maximum intensities in the two LIF bands (see text).

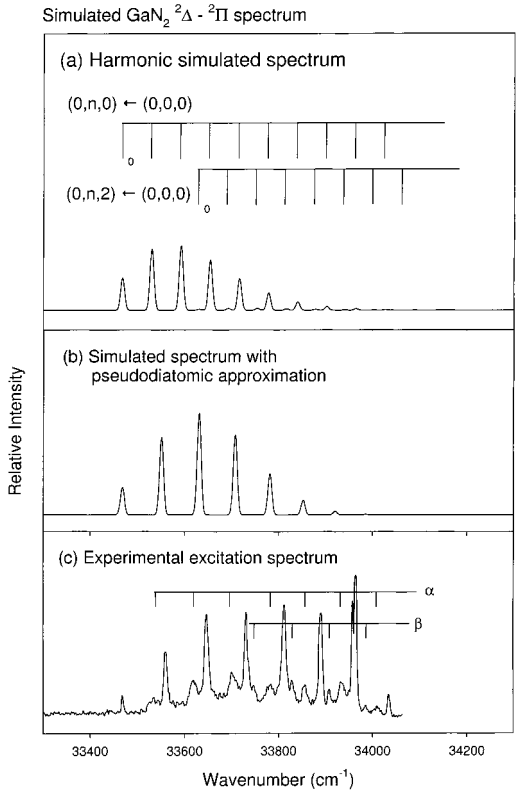

Figure 1. Simulated absorption spectra of the $^2\Delta \leftarrow \tilde{X}^2\Pi$ absorption of Ga•N_2 using computed Franck−Condon factors based on (a) the multidimensional harmonic model {employing the CASSCF(3,6)/6-311+G(3d)+sp3d and UCCSD(T)/6-311+G(3df) force constants of the $^2\Delta$ and $\tilde{X}^2\Pi$ states, respectively, and the RCCSD(T)/ECP[7s7p5d2f], aug-cc-pVTZ optimized geometries of the two states} and (b) the anharmonic pseudodiatomic model (see text for details). The LIF band with an observed onset at 33 468 cm^{-1} reported by Ellis et al. (from ref 3) is shown in (c) for comparison (the weak vibrational progressions labeled α and β are as from ref 3). It should be noted that, in the labeling scheme used for vibrational energy levels (ν_1, ν_2, ν_3), ν_1 and ν_2 refer to stretching modes and ν_3 refers to the deformation mode. ν_1 is the N−N stretching mode, ν_2 is the van der Waals stretching mode, and ν_3 is the bending mode.

ECP[7s7p5d2f], aug-cc-pVTZ level to be 3.92 eV (31617 cm^{-1}). This computed T_e value can be compared with the observed onset of the LIF band of 4.15 eV (33 468 cm^{-1}). The agreement between the computed and observed T_0/T_e values of within ca. 0.2 eV can be considered as reasonably good. In addition, the D_e value of the $^2\Delta$ state at the RCCSD(T)/ECP[11s10p6d5f3g], aug-cc-pVQZ//RCCSD(T)/ECP[7s7p5d2f], aug-cc-pVTZ level, including the full counterpoise correction[2] for BSSE, is calculated to be 1363.7 cm^{-1}. This computed value agrees very well with the D_0' value of 1270 ± 60 cm^{-1} derived from the Birge−Sponer plot in ref 3, supporting the assignment of the upper state to the $^2\Delta$ state of Ga•N_2. In summary, computed relative energies strongly support the assignment of the 33 468 cm^{-1} LIF band to the $^2\Delta \leftarrow \tilde{X}^2\Pi$ absorption of Ga•N_2.

The simulated spectra obtained with the computed multidimensional harmonic FCFs and the one-dimensional anharmonic FCFs are shown in Figure 1a,b), respectively. The observed spectrum from ref 3 is given in Figure 1c for comparison. For the sake of simplicity in the comparison, the T_0 positions of the simulated spectra were aligned to the position of the first observed peak of the LIF band at 33 468 cm^{-1}. First and foremost, it can be seen that both simulated spectra compare reasonably well with the observed spectrum. This is despite the slight differences between the computed and observed vibrational intervals. Therefore, on the basis of the computed vibrational frequencies, relative energies, and simulated spectra, it is concluded that the assignment of the LIF band at 33 468 cm^{-1} to the $^2\Delta \leftarrow \tilde{X}^2\Pi$ absorption of Ga•N_2 can be firmly established.

More careful comparisons between the simulated spectra and between the simulated and observed spectra lead to the following points for consideration.

(i) The simulated vibrational structure obtained on the basis of the multidimensional harmonic model has a longer stretching progression than that of the one-dimensional model. This is expected as the latter has included anharmonicities as mentioned above. Nevertheless, the spectral ranges covered by the two simulations are very similar and they are also very similar to that of the observed spectrum.

(ii) When the simulated and observed spectra are compared, both simulations assign the first observable peak to the (000)−(000) transition, confirming the tentative assignment given in ref 3 (see also later text). In this connection, the ν_{00} (or T_0) position of the $^2\Delta$ state is established to be 33 468 cm^{-1}. (In the labeling scheme used, ν_1 and ν_2 are stretching modes and ν_3 is a deformation mode.)

(iii) The comparison between the simulated and observed spectra shows clearly that the match is not perfect, particularly in the high-energy region of the band. The slight mismatch is separate from the slight differences between the computed and observed vibrational intervals and occurs in the overall shape of the simulated and observed vibrational envelopes. As the

transition energy is increased, both simulated absorption bands {Figure 1a,b) show an increase in the relative intensity to a maximum and then a gradual decrease. However, the relative intensities of the vibrational components in the high-energy region of the LIF band do not decrease with increasing energy as in the simulated spectrum (see Figure 1). With careful examination of the vibrational envelope of the LIF band at 33 468 cm^{-1}, there appear to be two band maxima (the third and fifth peaks in Figure 1c). In addition, the intensities of the high-energy vibrational components appear to decrease rather abruptly at the eighth peak of the LIF spectrum. These observations seem to suggest that variation in the dye laser intensity and the use of different laser dyes to cover this spectral region may have affected the observed vibrational envelope of this LIF band.

(iv) The iterative Franck−Condon analysis (IFCA) procedure, in which the GaN bond length of the upper state was varied systematically (see refs 12 and 15), was carried out by employing both the multidimensional harmonic FCF method and the one-dimensional pseudodiatomic method, with the hope of obtaining a better match between the simulated and observed spectra. However, the simulated vibrational envelopes show only one maximum and a gradual change in the relative intensities of neighboring vibrational components in all cases. No better match than those shown in Figure 1a,b with the observed LIF spectrum could be obtained with the IFCA procedure. It is therefore concluded that the discrepancies between the simulated and observed vibrational envelopes particularly in the high-energy region are probably due to some experimental problems in obtaining reliable component intensities, as suggested above.

(v) From the multidimensional harmonic FCF simulation, it can be seen that both the symmetric intermolecular stretching and bending modes are excited in the absorption, with the latter being excited in double quanta (Figure 1a). From Table 1, the computed harmonic vibrational frequencies of the bending mode obtained at different levels of calculation range from 81.2 to 120.7 cm^{-1}, values which are larger than the computed van der Waals stretching frequencies (62.1−71.3 cm^{-1}, respectively) in all cases. If the onset at 33 468 cm^{-1} of the LIF band is the 0−0 transition as concluded above, the first component involving excitation of the bending mode, (0,0,2), would then be expected to appear at an energy of ca. 162 cm^{-1} on the high-energy side of the first observed peak. In any case, the first component involving excitation of the bending mode should have a higher energy than the second component, (0,1,0), of the main Ga−N_2 stretching series. This would be true even if the bending mode were observed in single quantum excitations, as the computed Ga−N_2 stretching frequencies in the excited state are smaller than the computed bending frequencies in all cases. In this connection, the observed weak vibrational series labeled α by Ellis et al.,[3] which has its first observed component at ca. 60 cm^{-1} (estimated from the published spectrum[3]) on the high-energy side of the (0,0,0)−(0,0,0) component, cannot be due to the van der Waals bending mode as assigned by them. This conclusion is based on the assumption that the assignment of the first observed component to the (0,0,0)−(0,0,0) transition is correct (see also later text) and the relative magnitudes of the computed vibrational frequencies of the van der Waals stretching and bending modes are reliable. Following from this conclusion, our simulation in Figure 1a suggests that the weak vibrational series labeled β in the LIF band (Figure 1c) is probably due to the van der Waals bending mode excited in double quanta. The position of the first identifiable component in the β series is estimated from the published spectrum of Ellis et al.[3] to be ca. 280 cm^{-1} from the T_0 position. If this component is the (0,0,2) ← (0,0,0) transition, ν_3' would then have a value of ca. 140 cm^{-1}. However, it is also possible that the (0,0,2) ← (0,0,0) component is too weak to be observed. If the first observable component in the β series is (0,1,2), the (0,0,2) position can be estimated to be ca. 190 cm^{-1}. The corresponding ν_3' value would then be ca. 95 cm^{-1}. The latter assignment gives a ν_3' value which is almost identical to the ν_2' value. This is contrary to the computed results that the latter are consistently larger than the former. Ab initio results at present support the former assignment that the first observable vibrational component in the β series is the (002) ← (0,0,0) transition and ν_3', the bending frequency, has a value of 140 cm^{-1}.

(vi) With the best estimated D_0'' values of the $\tilde{X}^2\Pi_{3/2,1/2}$ states (320 and 95 cm^{-1}, respectively[1]), the measured ν_{00} value[3] (33 468 cm^{-1}), and available experimental atomic excitation energies (ΔE_{at}) of Ga,[16] the D_0' values of the upper state can be evaluated by employing the relationship $D_0' + \nu_{00} = D_0'' + \Delta E_{at}$. Ignoring the $^2\Delta_{5/2}$ spin−orbit state for the time being, which will be discussed later, there are two possible thermodynamic cycles to be used in applying this relationship. The first has ν_{00} of the Ga•N_2 $^2\Delta_{3/2}$ ← $\tilde{X}^2\Pi_{1/2}$ transition coupled with ΔE_{at} of the Ga $^2D_{3/2}$ ← $^2P_{1/2}$ transition (=34 782 cm^{-1}),[16] while the second uses ν_{00} for the $^2\Delta_{3/2}$ ← $\tilde{X}^2\Pi_{3/2}$ transition energy, with the $^2D_{3/2}$ ← $^2P_{3/2}$ transition (ΔE_{at} = 33 955 cm^{-1}).[16] For the first cycle with the $\tilde{X}^2\Pi_{1/2}$ initial state, the D_0' value is calculated to be 1409 cm^{-1}. For the second cycle with the $\tilde{X}^2\Pi_{3/2}$ initial state, the D_0' value is 807 cm^{-1}. From ref 3, the D_0' value was obtained from the Birge−Sponer plot to be 1270 ± 60 cm^{-1}, and in this work, the D_e' value for the $^2\Delta$ state of Ga•N_2 was calculated to be 1363.7 cm^{-1}. In a comparison of these D_0'/D_e' values, the first cycle using the ν_{00} value of 33 468 cm^{-1} corresponding to the $^2\Delta_{3/2}$ ← $\tilde{X}^2\Pi_{1/2}$ transition clearly gives a D_0' value which agrees better with those obtained from the Birge−Sponer plot and ab initio calculations than that from the second cycle. This leads to the conclusion that the initial state of the LIF band observed with an onset of 33 468 cm^{-1} is the $\tilde{X}^2\Pi_{1/2}$ state, not the $\tilde{X}^2\Pi_{3/2}$ state, as assigned in ref 3.

It is, however, worth considering in a little more detail, if the initial state of this LIF band would be the $\tilde{X}^2\Pi_{3/2}$ spin−orbit state, as assigned by Ellis et al.[3] Assuming the D_0' value of ca. 1270 cm^{-1} as derived from the Birge−Sponer plot and the appropriate D_0'' and ΔE_{at} values as used above, the ν_{00} value is evaluated to be ca. 33 000 cm^{-1}. This is 468 cm^{-1} lower than the measured onset of the band at 33 468 cm^{-1}. However, after making a particular effort to detect vibrational components below 33 468 cm^{-1}, Ellis et al. concluded that such additional bands, if they exist, must be at least 1 order of magnitude weaker than the 33 468 cm^{-1} band.[3] In addition, our spectral simulations suggest that the ν_{00} peak should be strong enough to be observed and the changes in the relative intensities of successive vibrational components should be gradual. Therefore, it seems certain that ν_{00} of this LIF band is 33 468 cm^{-1}. Hence the initial state cannot be the $\tilde{X}^2\Pi_{3/2}$ state, which would require a ν_{00} value of 33 000 cm^{-1} to complete the thermodynamic cycle. Alternatively, if the initial state were $\tilde{X}^2\Pi_{3/2}$, with the ν_{00} position of 33 468 cm^{-1}, as ascertained, the D_0' value is derived as 807 cm^{-1}, which is smaller than the D_0'/D_e' values obtained from the Birge−Sponer plot and ab initio calculations from this work by over 460 cm^{-1}.

In summary, it is reasonably conclusive that the initial state of the 33 468 cm^{-1} LIF band is not the $\tilde{X}^2\Pi_{3/2}$ state but the $\tilde{X}^2\Pi_{1/2}$ state, thus revising the initial state assignment of ref 3. With this revised initial state, the upper state has to be the $^2\Delta_{3/2}$

spin−orbit state, as a $^2\Delta_{5/2} \leftarrow \tilde{X}^2\Pi_{1/2}$ transition is forbidden on the basis of the selection rule of $\Delta\Omega = 0, \pm 1$. The LIF band at 33 468 cm^{-1} is therefore assigned to the $^2\Delta_{3/2} \leftarrow \tilde{X}^2\Pi_{1/2}$ Ga•N_2 transition in the present study.

(vii) Last, what remains unassigned in the 33 468 cm^{-1} LIF band is the weak and also diffuse progression labeled α in ref 3. We propose to assign this series to the $^2\Delta_{5/2,3/2} \leftarrow \tilde{X}^2\Pi_{3/2}$ transitions of Ga•N_2. The reasons for suggesting this assignment are as follows. First, the similar observed vibrational intervals of the α series and the main series suggest that they are very likely accessing the same upper state. Second, the $\tilde{X}^2\Pi_{3/2}$ state can access the two spin−orbit states, $^2\Delta_{5/2,3/2}$, which are expected to be close in energy (the spin−orbit splitting was estimated to be 2.5 cm^{-1} in ref 3, and the Ga $^2D_{5/2,3/2}$ spin−orbit splitting[16] is ca. 7 cm^{-1}). We suggest that the diffuseness of the vibrational components in the progression labeled α is probably due to unresolved spin−orbit splitting in the upper state. Third, since the $\tilde{X}^2\Pi_{3/2}$ state is higher in energy than the $\tilde{X}^2\Pi_{1/2}$ state, it is reasonable to expect that the former state has a smaller population than the latter. Hence, LIF bands originating from the former state are expected to be weaker, as observed with the α series. Fourth, regarding the initial state, the $^2\Pi_{3/2}$ state was calculated to be 567 cm^{-1} above the $\tilde{X}^2\Pi_{1/2}$ state in our earlier work.[1] Together with the ν_{00} value of the $^2\Delta_{3/2} \leftarrow \tilde{X}^2\Pi_{1/2}$ transition of 33 468 cm^{-1}, the ν_{00} of the $^2\Delta_{3/2} \leftarrow \tilde{X}^2\Pi_{3/2}$ transition of Ga•N_2 is evaluated to be 32 901 cm^{-1}. With the appropriate D_0'' and ΔE_{at} values as used above, the D_0' value of the $^2\Delta_{3/2}$ states is calculated with the relationship given above to be 1374 cm^{-1}. This value agrees reasonably well with the computed D_e' value of 1363.7 cm^{-1} and the D_0' value of 1409 cm^{-1} derived above from considering the $^2\Delta_{3/2} \leftarrow \tilde{X}^2\Pi_{1/2}$ transition. In this connection, with the present proposed assignment of the α series, the ν_{00} positions of the $^2\Delta_{5/2,3/2} \leftarrow \tilde{X}^2\Pi_{3/2}$ transitions are estimated to be at ca. 32 900−33 000 cm^{-1}. These values are ca. 500 cm^{-1} lower in energy than the observed onset of the $^2\Delta_{3/2} \leftarrow \tilde{X}^2\Pi_{1/2}$ LIF band (33 468 cm^{-1}). It appears that the $^2\Delta_{5/2,3/2} \leftarrow \tilde{X}^2\Pi_{3/2}$ transitions of Ga•N_2 are too weak to be observed. This is probably due partly to a low population in the initial state and partly to poor Franck−Condon factors in the region of the band onset. These poor Franck−Condon factors suggest that the GaN bond length changes in the $^2\Delta_{5/2,3/2} \leftarrow \tilde{X}^2\Pi_{3/2}$ transitions are larger than that in the $^2\Delta_{3/2} \leftarrow {}^2\Pi_{1/2}$ transition.

$^4\Sigma^-$ State and LIF Band at 37 633 cm^{-1}. First, the vertical excitation energy (VEE) for the $^4\Sigma^- \leftarrow \tilde{X}^2\Pi$ transition is considered. From Table 2, it can been seen that the computed VEEs are more sensitive to the levels of calculation than those of the $^2\Delta \leftarrow \tilde{X}^2\Pi$ transition. The computed VEE values increase with the levels of calculation to a maximum of 4.39 eV {35411 cm^{-1}; at the RCCSD(T)/ECP[11s10p6d5f3g], aug-cc-pVQZ level}. This is the computed VEE which is closest to the experimental value of 4.73 eV (38 123 cm^{-1}; the estimated position of the sixth peak in the LIF band from Figure 3 in ref 3). The agreement between the computed and observed VEEs of 0.34 eV can be considered as fair, but it is not as good as that for the $^2\Delta \leftarrow \tilde{X}^2\Pi$ transition and also slightly worse than the expected accuracy from high-level ab initio calculations of within 0.2 eV for relative electronic energies.

The computed geometrical parameters and harmonic vibrational frequencies of the $^4\Sigma^-$ state of Ga•N_2 are summarized in Table 3. Although the computed geometrical parameters vary with the levels of calculation and the calculated GaN bond lengths range from 1.81 to 2.09 Å, the computed GaN bond lengths are consistently and significantly shorter than those of the $\tilde{X}^2\Pi$ and the $^2\Delta$ states (see ref 1 and Table 1, respectively). From the computed GaN bond lengths, it is obvious that the $^4\Sigma^-$ state is not a weakly bound van der Waals state, like the $\tilde{X}^2\Pi$ and the $^2\Delta$ states. Similarly, although the computed harmonic vibrational frequencies of the intermolecular modes of the $^4\Sigma^-$ state cover a fairly wide range (from 200 to 600 cm^{-1}; see Table 3), they are considerably larger than those of the $\tilde{X}^2\Pi$ and the $^2\Delta$ states (ref 1 and Table 1). On the basis of the calculated GaN bond lengths and intermolecular vibrational frequencies, the $^4\Sigma^-$ state of Ga•N_2 is a well-bound state; actually, it is a charge-transfer state, and this will be discussed later. More significantly, the calculated vibrational frequencies are considerably larger than the measured vibrational intervals of 80 cm^{-1} in the LIF band at 37 633 cm^{-1}.

TABLE 3: Optimized Geometrical Parameters and Calculated Harmonic Vibrational Frequencies (cm^{-1}) of the Lowest $^4\Sigma^-$ State ($...\sigma^1\pi^2$) of Ga•N_2 at Different Levels of Calculation

method	GaN/Å	NN/Å	ω_1(NN)	$\omega_2(\sigma)$	$\omega_3(\pi)$
GRHF/SV+diff+polarization[a]	2.0877	1.0785	2663.8	230.8	326.1
CASSCF(3,6)/6-311+G(2d)	2.0877	1.0699	2925.0	211.1	712.2
B3LYP/6-311+G(2d)	1.8223	1.1438	1812.7	486.8	317.7
B3LYP/6-311+G(3df)	1.8182	1.1437	1822.8	489.9	328.8
MP2/6-311+G(2d)	2.0786	1.0854	3313.8	222.5	290.5
MP2/6-311+G(3df)	2.0478	1.0860	3250.4	241.7	307.3
QCISD/6-311+G(2d)[b]	1.9340	1.1167			
QCISD/6-311+G(3df)[b]	1.9215	1.1178			
CCSD(T)/6-311+G(2d)	1.9297	1.1204	1993.1	620.5	305.2; 316.9
CCSD(T)/6-311+G(3df)[c]	1.8174	1.1562			
CCSD(T)/lanl2[8s6p5d2f][d]	1.8484	1.1378	1880.3	415.9	338.1; 339.2

[a] See text for the basis set used. [b] Problems with numerical second derivation calculations, giving unrealistic frequencies. [c] Not optimized geometry; search unable to find next point. At this geometry and level of calculation, the $^4\Sigma^-$ state is 75.2 kcal/mol above the $\tilde{X}^2\Pi$ state. [d] The ECP basis is for Ga [from ref 1; also see text; for N, the 6-311+G(3df) basis has been employed]. At this level of calculation the $^4\Sigma^-$ state is 68.3 kcal/mol above the $\tilde{X}^2\Pi$ state.

Multidimensional harmonic FCF calculations and spectral simulations were carried out for the **$^4\Sigma^- \leftarrow \tilde{X}^2\Pi$** absorption, employing UCCSD(T)/lanl2[8s6p5d2f],6-311+G(3df) (see Table 3) and UCCSD(T)/6-311+G(3df) (from ref 1) geometries and force constants for the $^4\Sigma^-$ and $\tilde{X}^2\Pi$ states, respectively. However, with a large difference of more than 1 Å between the calculated equilibrium Ga−N bond lengths of the two states and the small computed Ga−N_2 vibrational intervals, the computed FCFs did not reach a maximum even on excitation to the 170th vibrational level of the upper state in the Ga−N symmetric stretching mode. (The limit of the harmonic FCF code used is 171 vibrational levels at present.) With the IFCA procedure, assuming a longer Ga−N bond length of 2.5 Å in the upper state, the simulated spectrum peaked at ca. $\nu_2 = 100$ and covered a very long spectral range of over 1 eV (8000 cm^{-1}). Although the simulated spectrum with the computed minimum-energy geometries of the two states has not been obtained, it is expected that it will be very different from the LIF band observed at 37 633 cm^{-1}. On the basis of the computed harmonic vibrational frequencies and spectral simulation, it is concluded that the observed LIF band at 37 633 cm^{-1} cannot be assigned to the $^4\Sigma^- \leftarrow \tilde{X}^2\Pi$ transition.

Other Low-Lying Quartet States of Ga•N_2. In search of a suitable candidate for the upper state of the 37 633 cm^{-1} LIF band, a number of low-lying, linear, and T-shaped quartet states have been investigated in addition to the $^4\Sigma^-$ state. The results from some initial calculations on these states are given in Tables 4 and 5. First, it is anticipated that the linear $^4\Pi$ state with the $...\sigma^1\pi^1\sigma^1$ electronic configuration [corresponding to Ga $(4s\sigma)^1$-

TABLE 4: Optimized Geometrical Parameters and Calculated Harmonic Vibrational Frequencies (cm^{-1}) of Low-Lying Quartet States of Ga•N_2 (T-shape C_{2v} Structures) at the MP2/6-311+G(2d) and QCISD/6-311+G(2d) Levels of Calculation

state	GaN/Å	NN/Å	NGaN/deg	$\omega(a_1)$	$\omega(a_1)$	$\omega(b_2)$
			MP2			
1^4A_1	3.5329	1.2214	19.9	1670.6	26.0i	124.7i
1^4B_1	1.8950	1.3424	41.5	1159.4	558.3	405.8
2^4B_1	4.8740	1.1060	13.0	2230.6	19.2	204.2
1^4B_2	4.9728	1.1060	12.8	2230.9	17.0	12.0i
2^4B_2	2.2864	1.3077	33.2	1922.8	358.2	504.4
1^4A_2	2.2401	1.1451	29.6	2495.1	374.8	638.7
2^4A_2	2.7253	1.1133	23.6	2144.3	20.0	125.1
			QCISD			
1^4A_1	3.6673	1.2119	19.0	1740.5	38.4	97.1i
1^4B_1	1.9523	1.4035	68.9	916.3	564.4	102.3i
2^4B_1	4.9351	1.0933	12.7	2415.7	18.2	3.4i
1^4B_2	4.9741	1.0934	12.6	2415.3	17.7	12.3
2^4B_2	2.1235	1.2253	33.5	1301.9	366.6	184.5i
1^4A_2	2.1393	1.1577	31.4	1729.5	309.2	233.7
2^4A_2	*a*					

[a] Optimization not converged after 70 points from the initial MP2-optimized geometry.

TABLE 5: Open-Shell Electronic Configurations, Relative Energies[a] (E_{rel} in kcal/mol), and Computed Charge (q) and Spin (s) Densities of Low-Lying Quartet States of Ga•N_2 at the MP2/6-311+G(2d) and QCISD/6-311+G(2d) Levels of Calculation

state[b]	confign	E_{rel}	q_{Ga}	q_N	s_{Ga}	s_N
			MP2			
$1^4\Sigma^-$	$(\sigma)^1(\pi)^2$	74.6	0.13	0.05; −0.18	2.95	−0.41; 0.45
$1^4\Pi$	$(\sigma)^1(\pi)^1(\sigma)^1$	87.9	−0.01	−0.06; 0.07	3.00	−0.01; 0.00
1^4A_1	$(a_1)^1(b_2)^1(b_2)^1$	173.0	−0.03	0.01	1.01	1.00
1^4B_1	$(a_1)^1(b_2)^1(a_2)^1$	87.1	0.96	−0.48	0.65	1.18
2^4B_1	$(a_1)^1(b_1)^1(a_1)^1$	87.8	−0.01	0.00	3.00	−0.00
1^4B_2	$(a_1)^1(b_2)^1(a_1)^1$	87.9	−0.01	0.00	3.00	0.00
2^4B_2	$(a_1)^1(b_1)^1(a_2)^1$	120.3	0.53	−0.27	1.82	0.59
1^4A_2	$(a_1)^1(b_1)^1(b_2)^1$	85.2	0.23	−0.11	2.63	0.19
2^4A_2	$(a_1)^1(b_2)^1(b_1)^1$	88.4	−0.05	0.03	3.00	0.00
			QCISD			
$1^4\Sigma^-$	as above	76.7	0.25	−0.15; −0.10	2.82	−0.68; 0.86
$1^4\Pi$		93.44	−0.01	−0.06; 0.07	3.00	−0.01; 0.00
1^4A_1		173.8	−0.02	0.01	1.01	1.00
1^4B_1		87.3	0.88	−0.44	0.41	1.30
2^4B_1		93.4	−0.01	0.00	3.00	−0.00
1^4B_2		93.4	−0.01	0.00	3.00	−0.00
2^4B_2		129.4	0.60	−0.30	1.90	0.55
1^4A_2		91.1	0.42	−0.21	2.34	0.33
2^4A_2		*c*				

[a] With respect to the $\tilde{X}^2\Pi$ state. [b] States in italics are true minima, with all real frequencies (see Table 3). [c] Optimization not converged after 70 points from the initial MP2-optimized geometry.

$(4p\pi)^1(4p\sigma)^1$] would be slightly higher in energy than the $^4\Sigma^-$ state with the $...\sigma^1\pi^2$ electronic configuration [corresponding to Ga $(4s\sigma)^1(4p\pi)^2$]. Since the computed VEEs of the $^4\Sigma^- \leftarrow \tilde{X}^2\Pi$ transition are consistently slightly smaller than the observed value, the $^4\Pi$ state would then be an obvious candidate for the upper state of the 37 633 cm^{-1} LIF band; hence, it is considered first. The computed VEEs for the $^4\Pi \leftarrow \tilde{X}^2\Pi$ absorption are given in Table 2, and they agree with the experimental value to within 0.26 eV. This agreement between the computed and observed VEE values is better than that for excitation to the $^4\Sigma^-$ state.

The optimized geometrical parameters and computed harmonic vibrational frequencies of the $^4\Pi$ state of Ga•N_2 obtained at different levels of calculation are summarized in Table 6. From Table 6, the computed GaN bond lengths are consistently very long (ca. 5.0 Å). Although there were SCF convergence

TABLE 6: Optimized Geometries and Harmonic Vibrational Frequencies (cm^{-1}) of the $^4\Pi$ State ($...\sigma^1\pi^1\sigma^1$) of Ga•N_2 at Different Levels of Calculations

method	GaN/Å	NN/Å	ω_1(NN)	$\omega_2(\sigma)$	$\omega_3(\pi)$
MP2/6-311+G(2d)	4.9702	1.1061	2229.8	15.2	24.8; 28.4
MP2/6-311+G(3df)	5.0572	1.1053	2247.5	11.4	6.4i; 15.2
QCISD/6-311+G(2d)	5.0009	1.0934	2414.8	15.0	18.9; 23.1
CCSD(T)/6-311+G(2d)[a]	4.9999	1.0981			
CCSD(T)/6-311+G(3df)[b]	5.0163	1.0974			

[a] SCF convergence failure in the numerical second derivative calculation; at this level of calculation, the $^4\Pi$ state is 94.0 kcal/mol above the $\tilde{X}^2\Pi$ state. [b] SCF converged to the lower $...\sigma^1\pi^2$ $^4\Sigma^-$ state in the numerical second derivative calculation; 94.8 kcal/mol above the $\tilde{X}^2\Pi$ state at this level of calculation.

problems in the numerical second derivative calculations at the UCCSD(T) level and these frequency calculations were not completed, the computed harmonic vibrational frequencies of the intermolecular modes at the MP2 and QCISD levels are consistently very small (<30 cm^{-1}; Table 6). From the computed Ga•N bond lengths and the intermolecular vibrational frequencies, it is clear that the $^4\Pi$ state is a very weakly bound state, significantly more weakly bound than the $\tilde{X}^2\Pi$ state. If the computed intermolecular vibrational frequencies are compared with the measured vibrational intervals of ca. 80 cm^{-1} of the 37 633 cm^{-1} LIF band, the agreement cannot be considered as good. As with the $^4\Sigma^-$ state above, FCF calculations and spectral simulations were carried out for the $^4\Pi \leftarrow \tilde{X}^2\Pi$ absorption of Ga•N_2. The QCISD/6-311+G(2d) geometry and force constants were used for the $^4\Pi$ state (see Table 6). Similar to the $^4\Sigma^-$ state, the same problem of not being able to reach the band maximum at the 170th vibrational level of the upper state in the Ga−N symmetric stretching mode was encountered. With an even larger difference in the computed equilibrium Ga−N bond lengths between the $^4\Pi$ and $\tilde{X}^2\Pi$ states than between the $^4\Sigma^-$ and $\tilde{X}^2\Pi$ states, it is expected that the simulated absorption spectrum between the former two states will have an even longer stretching progression than that between the latter two states. The $^4\Pi \leftarrow \tilde{X}^2\Pi$ absorption spectrum is therefore expected to be very different from the observed LIF band at 37 633 cm^{-1}. In summary, on the basis of the calculated VEE, the $^4\Pi$ state is a more likely candidate for the assignment of the upper state of the 37 633 cm^{-1} LIF band than the $^4\Sigma^-$ state. However, on the basis of the computed vibrational frequencies and the expected simulated spectrum, the upper state of this LIF band cannot be assigned to the $^4\Pi$ state.

Concerning other quartet states considered in the present study, they will not be discussed in detail. However, it can be seen from Tables 4 and 5 that, in general, none of these quartet states can be assigned to the upper state of the LIF band at 37 633 cm^{-1}. If these states are in the correct energy region, they are either very weakly bound van der Waals states, like the $^4\Pi$ state, or well-bound charge-transfer states, like the $^4\Sigma^-$ state. Their computed intermolecular stretching vibrational frequencies are either too small (less than 40 cm^{-1}) or too large (larger than 300 cm^{-1}), when compared with the measured vibrational intervals of the LIF band at 37 633 cm^{-1}. Similar to the $^4\Sigma^-$ and $^4\Pi$ states discussed above, the computed GaN bond lengths of these quartet states differ significantly from that of the $\tilde{X}^2\Pi$ state. In addition, it is expected that an absorption band from the linear $\tilde{X}^2\Pi$ state to a quartet state with a T-shaped structure would consist of a long and complex vibrational envelope, because of the large geometry differences between the two states. In summary, none of the quartet states considered here can be assigned to the upper state of this LIF band.

TABLE 7: Optimized Geometrical Parameters and Harmonic Vibrational Frequencies (cm^{-1}) of the ...$(a_1)^1(b_2)^1(a_2)^1$ $^4B_1$ State of $Ga{\cdot}N_2$ at Different Levels of Calculation

method	GaN/Å	NN/Å	NGaN/deg	$\omega_1(a_1)$	$\omega_2(a1)$	$\omega_3(b_2)$
MP2/6-311+G(2d)	1.8950	1.3424	41.5	1159.4	558.3	405.8
MP2/6-311+G(3df)	1.8950	1.3407	41.4	1235.2	580.2	411.8
QCISD/6-311+G(2d)	1.9523	1.4035	42.1	916.3	564.4	102.3i
QCISD/6-311+G(3df)[a]	1.9486	1.4002	42.1			
CCSD(T)/6-311+G(2d)	1.9482	1.4094	42.4	888.4	570.3	230.4
CCSD(T)/6-311+G(3df)[b]	1.9456	1.4050	42.3	925.2	586.1	252.5

[a] Numerical second derivatives calculations failed. [b] The $^4B_1$ state is 78.1 kcal/mol above the $\tilde{X}^2\Pi$ state at the CCSD(T)/6-311+G(3df) level of calculation.

TABLE 8: Optimized Geometrical Parameters and Harmonic Vibrational Frequencies (cm^{-1}) of the ...$(a_1)^1(b_1)^1(a_2)^1$ $^4B_2$ State of $Ga{\cdot}N_2$ at Different Levels of Calculation

method	GaN/Å	NN/Å	NGaN/deg	$\omega_1(a_1)$	$\omega_2(a_1)$	$\omega_3(b_2)$
MP2/6-311+G(2d)	2.2864	1.3077	33.2	1922.8	358.2	504.4
MP2/6-311+G(3df)	2.2927	1.3081	33.1	1923.4	369.2	429.0
QCISD/6-311+G(2d)	2.1235	1.2253	33.5	1301.9	366.6	184.5i
QCISD/6-311+G(3df)	2.1203	1.2288	33.7	1105.1	389.8	295.4
CCSD(T)/6-311+G(2d)[a]	2.3304	1.2965	32.3			
CCSD(T)/6-311+G(3df)[b]	2.3342	1.2970	32.3			

[a] SCF convergence problems in the numerical second derivative calculations. [b] SCF convergence problems in the numerical second derivative calculations. The $^4B_2$ state is 119.6 kcal/mol above the $\tilde{X}^2\Pi$ state at the CCSD(T)/6-311+G(3df) level of calculation.

TABLE 9: Optimized Geometrical Parameters and Harmonic Vibrational Frequencies (cm^{-1}) of the ...$(a_1)^1(b_2)^1(b_1)^1$ $^4A_2$ State of $Ga{\cdot}N_2$ at Different Levels of Calculation

method	GaN/Å	NN/Å	NGaN/deg	$\omega_1(a_1)$	$\omega_2(a_1)$	$\omega_3(b_2)$
MP2/6-311+G(2d)	2.2401	1.1451	29.6	2495.1	374.8	638.7
MP2/6-311+G(3df)	2.2270	1.1441	29.8	2145.4	379.0	585.9
QCISD/6-311+G(2d)	2.1393	1.1577	31.4	1729.5	309.2	233.7
QCISD/6-311+G(3df)	2.1213	1.1598	31.7	1736.9	332.5	234.1
CCSD(T)/6-311+G(2d)	2.1487	1.1627	31.4	1710.6	301.0	308.6
CCSD(T)/6-311+G(3df)[a]	2.1291	1.1660	31.8	1703.3	326.2	308.6

[a] The $^4A_2$ state is 88.0 kcal/mol above the $\tilde{X}^2\Pi$ state at the CCSD(T)/6-311+G(3df) level.

Low-Lying Charge-Transfer Quartet States of $Ga{\cdot}N_2$. From Tables 4 and 5, it can been seen that, in addition to the linear $^4\Sigma^-$ state of $Ga{\cdot}N_2$, there are at least three T-shaped quartet states, namely the 1^4B_1, 2^4B_2, and 1^4A_2 states, which are well-bound charge-transfer states with relatively short computed GaN bond lengths of ca. 2.0 Å. These charge-transfer states were studied further at higher levels of calculation than those given in Tables 4 and 5. Their optimized geometrical parameters and computed harmonic vibrational frequencies are summarized in Tables 7−9. The consistency of these results obtained at different levels of calculation shows their reliability and supports strongly the existence of these charge-transfer quartet $Ga{\cdot}N_2$ states.

From Table 5, it can be seen that the computed charge and spin density on each atomic center vary from state to state and they differ slightly at different levels of calculation. Nevertheless, it is clear that the $^4\Sigma^-$, 1^4B_1, 2^4B_2, and 1^4A_2 states are charge-transfer states. In each case, the computed charge density on Ga is significantly larger than zero (but less than one), suggesting significant charge transfer from Ga to N_2. The computed spin densities on Ga and N of these states are nonintegers and significantly larger than zero, suggesting delocalization of unpaired electron spins and a certain degree of covalent interaction between Ga and N_2. It can also been seen that the computed N−N bond lengths of these states are lengthened and the calculated N−N vibrational frequencies decreased, when compared with those of an isolated dinitrogen molecule. These computed results suggest significant activation in the dinitrogen molecule arising from interaction with the Ga atom.

SCHEME 1

Considering the HOMOs and LUMOs of isolated Ga and N_2, respectively, the HOMOs of Ga, $4s^24p^1$, become $\sigma^2\pi^1$ in the ground state of linear $Ga{\cdot}N_2$. The Ga 4pπ molecular orbitals can interact in a bonding fashion with the LUMOs, π_g*, of N_2 in the formation of the complex, as shown in Scheme 1.

This orbital interaction is bonding between Ga and N_2 and is expected to reduce the Ga−N bond length. At the same time, the N−N bond length is expected to be lengthened, because of the involvement of the N_2 π* antibonding orbital. However, such orbital interaction between Ga and N_2 is negligibly small in the $\tilde{X}^2\Pi$ state of $Ga{\cdot}N_2$. Nevertheless, it becomes strong when an electron is excited from the highest doubly occupied (essentially Ga 4s) σ molecular orbital to the set of the highest singly occupied (originally Ga 4p) π molecular orbitals to form the $^4\Sigma^-$ state. On one hand, the removal of an electron from the Ga 4sσ orbital reduces the electron−electron repulsion between Ga and N_2 along the intermolecular axis. On the other hand, in the excited $^4\Sigma^-$ state, with the $\sigma^1\pi^2$ configuration, the participation of the N_2 π_g* orbitals in the π HOMOs becomes significantly stronger than in the $\tilde{X}^2\Pi$ state. Both effects lead to a shorter Ga−N bond length and a longer N−N bond length in the $^4\Sigma^-$ state than in the $\tilde{X}^2\Pi$ state. In addition, there is significant charge transfer from Ga to N_2 via the two electrons originally on Ga, now occupying the pair of delocalized π HOMOs. The resulting electrostatic attraction in the polarized, $Ga^{\delta+}{\cdot}N_2^{\delta-}$ state also increases the bonding of the system, giving a shorter Ga−N bond length. In summary, it is the combined

SCHEME 2

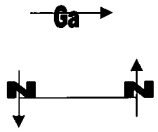

and inter-relating effects of the promotion of an electron from Ga $4s\sigma^2$ to $4p\pi^1$, the interaction between the π HOMOs of Ga and the π^* LUMOs of N_2, and the electrostatic attraction resulting from charge transfer from Ga to N_2 which lead to a short GaN bond length and large intermolecular vibrational frequencies of the $^4\Sigma^-$ state of Ga•N_2. Both bonding interaction via delocalization of molecular orbitals and the resulting electrostatic attraction strengthen the bonding between Ga and N_2 in the $^4\Sigma^-$ state considerably, and there is now significant interaction between the metal center and the dinitrogen molecule in this state.

For the T-shaped charge-transfer quartet states, the in-plane Ga $4p(b_2)$ and the N_2 $\pi^*(b_2)$ orbitals can have bonding interaction, as shown in Scheme 2.

This is in a way similar to the π HOMOs in the linear $^4\Sigma^-$ state considered above in that the metal−dinitrogen orbital interaction is bonding in character. The participation of the metal $p(b_2)$ orbital in this molecular orbital reduces the antibonding character of the N_2 $\pi^*(b_2)$ antibonding orbital. Also, similar to the linear structure discussed above, such interaction is negligibly small in the T-shaped $^2B_1$ state (see ref 1). The excitation of an electron from Ga $4s(a_1)^2$ to a Ga 4p orbital is required to reduce the in-plane electron−electron repulsion and involve the kind of orbital interaction shown in Scheme 2. The occupation of this b_2 molecular orbital in a T-shaped quartet state by an electron also leads to electrostatic attraction resulting from charge transfer from Ga and N_2, similar to the linear π molecular orbital discussed above. In addition, excitation of an electron from the Ga $4s(a_1)$ orbital to the vacant N_2 $\pi^*(a_2)$ orbital leads to the transfer of one electron from Ga to N_2, resulting in an ion-pair state with strong electrostatic attraction. The computed charge and spin densities and the stability of the three T-shaped charge-transfer states considered here can be understood from their electronic configurations in terms of the above considerations.

Concluding Remarks

High-level ab initio calculations were performed on the $^2\Delta$ state and a number of low-lying quartet states of Ga•N_2. FCF calculations were carried out on selected electronic absorptions. With the aid of computed relative energies, harmonic vibrational frequencies, and spectral simulations based on computed FCFs, the LIF band observed by Ellis et al.[3] at 33 468 cm^{-1}, and assigned by them to the $^2\Delta \leftarrow \tilde{X}^2\Pi_{3/2}$ transition, is assigned to the $^2\Delta_{3/2} \leftarrow \tilde{X}^2\Pi_{1/2}$ transition of Ga•N_2. This assignment confirms that the molecular carrier of this LIF band is Ga•N_2 and agrees with Ellis et al. regarding the assignments of the symmetries of the lower and upper electronic states. However, the spin−orbit designations of both states have been revised. In addition, the observed onset of this LIF band is confirmed to be the ν_{00} position, hence establishing the T_0 value of the transition. Following from this conclusion, the assignments of the observed vibrational transitions including the assignments of the weaker series in this band labeled as α and β by Ellis et al. are also revised.

A considerable effort has been made to assign the LIF band observed at 37 633 cm^{-1} by Ellis et al. without success. Our calculations and spectral simulations clearly do not support the assignment made by Ellis et al. of this band to the $^4\Sigma^- \leftarrow {}^2\Pi$ transition of Ga•N_2. Despite consideration of a large number of low-lying quartet states of Ga•N_2, a suitable candidate cannot be found for the upper state of this band. The identity of the molecular carrier of this LIF band is still therefore in doubt.

SCHEME 3

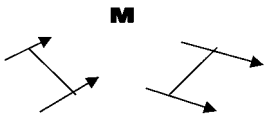

In the search for a suitable candidate for the upper state of the LIF band at 37 633 cm^{-1}, a number of linear and T-shaped charge-transfer quartet states of Ga•N_2 have been investigated for the first time. In these charge-transfer states, there is significant orbital mixing and electrostatic interaction between Ga and N_2, which lead to short computed Ga−N bond lengths and large intermolecular vibrational frequencies. At the same time, the computed N−N bond lengths are significantly lengthened, while the N−N stretching frequencies decrease, in comparison with those of isolated N_2. All these computed results show strong interaction between the metal center and the dinitrogen molecule in these charge-transfer states of Ga•N_2. In this connection, two points should be mentioned. First, in consideration of metal−dinitrogen interaction and/or N_2 activation by a metal center, attention has been focused mainly on transition metals.[17] This is the first time that a p-block metal has been demonstrated to have significant interaction with a dinitrogen molecule in a number of low-lying quartet states.

Second, the kind of orbital interaction considered above may lead to possible application in obtaining M•N_n systems, which may be used as precursors of high energy density materials (HEDM). Polynitrogen species, N_n, have received considerable attention as possible candidates of HEDM recently (for examples, refs 4, and 18−24 and references therein). The instability of these species, the low barrier to dissociation in particular (for examples, refs 19, 20, 22, and 25), seems to be a major difficulty for these species to have real applications. Following from the above discussion, an M•N_4 ring system, where M is a p-block metal with a ground-state open-shell s^2p^1 electronic configuration like Ga, is considered here as an illustration. The major destabilizing effect in forming a five-membered ring of M•N_4 comes from the pair of HOMOs, which are the N_2 π/N_2 π antibonding combinations (though bonding in N_2). The in-plane molecular orbital of the pair, with b_2 symmetry in the C_{2v} point group, is shown in Scheme 3. The corresponding out-of-plane molecular orbital is of a_2 symmetry. Excitation of an electron from either of these two molecular orbitals would reduce the destabilizing effect from these molecular orbitals of N_2–N_2 antibonding interaction.

On the other hand, the pair of LUMOs of N_2 π^* + N_2 π^* bonding combinations (though antibonding in N_2) would, with the participation of the appropriate metal p orbitals, stabilize ring formation, as shown in Scheme 4. The occupation of either molecular orbitals (in-plane a_1 or out-of-plane b_1) of this pair of LUMO bonding combinations by an electron would stabilize the ring, shorten the intermolecular N_2–N_2 and M−N bond lengths, and lengthen the intramolecular N−N bond lengths. On the basis of the above considerations, it is anticipated that, with the appropriate electronic configurations, some quartet states of the M•N_4 ring system should be reasonably stable with a significant energy well depth. Preliminary calculations on Al•

SCHEME 4

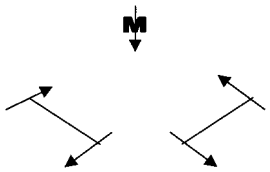

N_4 indeed show the existence of such quartet states. Further calculations on the ring structure and also other structures of $Al{\cdot}N_4$ are under way, and their results will be reported elsewhere.

Acknowledgment. Financial support from DERA (Fort Halstead, U.K.) and computational resources from EPSRC via the UK Computational Chemistry Facility are gratefully acknowledged. The authors are also grateful for support from the Research Grant Council (RGC) of the Hong Kong Special Administrative Region (Project Nos. POLYU 5180/99P and POLYU 5187/00P) and the Research Committee of the Hong Kong Polytechnic University. Dr. Andrew M. Ellis (Leicester University) is acknowledged for valuable discussions.

References and Notes

(1) Lee, E. P. F.; Dyke, J. M. *J. Phys. Chem. A* **2000,** *104*, 11810.

(2) Boys, S. F.; Bernardi, F. *Mol. Phys.* **1970**, *19*, 553.

(3) Greetham, G. M.; Hanton, M. J.; Ellis, A. M. *Phys. Chem. Chem. Phys.* **1999**, *1*, 2709.

(4) For examples: Bartlett, R. J. *Chem. Ind.* **2000**, *140*.

(5) Frisch, M. J.; Trucks, G. W.; Schlegel, H. B.; Scuseria, G. E.; Robb, M. A.; Cheeseman, J. R.; Zakrzewski, V. G.; Montgomery, J. A.; Stratmann, R. E.; Burant, J. C.; Dapprich, S.; Millam, J. M.; Daniels, A. D.; Kudin, K. N.; Strain, M. C.; Farkas, O.; Tomasi, J.; Barone, V.; Cossi, M.; Cammi, R.; Mennucci, B.; Pomelli, C.; Adamo, C.; Cliffoird, S.; Ochterski, J.; Petersson, G. A.; Ayala, P. Y.; Cui, Q.; Morokuma, K.; Malick, D. K.; Rabuck, A. D.; Raghavachari, K.; Foresman, J. B.; Cioslowski, J.; Ortiz, J. V.; Stefanov, B. B.; Liu, G.; Liashenko, A.; Piskorz, P.; Komaromi, I.; Gomperts, R.; Martin, R. L.; Fox, D. J.; Keith, T.; Al-Laham, M. A.; Peng, C. Y.; Nanayakkara, A.; Gonzalez, C.; Challacombem, M.; Gill, P. M. W.; Johnson, B. G.; Chen, W.; Wong, M. W.; Andres, J. L.; Head-Gordon, M.; Replogle, E. S.; Pople, J. A. *Gaussian98*; Gaussian, Inc.: Pittsburgh, PA, 1998.

(6) GAMESS-UK is a package of ab initio programs written by M. F. Guest, J. H. van Lenthe, J. Kendrick, K. Schofel, and P. Sherwood. with contributions from R. D. Amos, R. J. Buenker, M. Dupuis, N. C. Handy, I. H. Hiller, P. J. Knowles, V. Bonacic-Koutecky, W. von Niessen, R. J. Harrison, A. P. Rendell, V. R. Saunders, and A. J. Stone., The package is derived from the original GAMESS code due to M. Dupuis, D. Spangler, and J. Wendoloski, NRCC Software Catalog, Vol. 1, Program No QG01 (GAMESS), 1980.

(7) Dunning, T. H., Jr.; Hay, P. J. *Modern Theoretical Chemistry*; Schaefer, H. F., Ed.; Plenum: New York, 1977; Vol.3, 1.

(8) Knowles, P. J.; Hampel, C.; Werner, H. J. *J. Chem. Phys.* **1993**, *99*, 5219.

(9) MOLPRO is a package of ab initio programs written by H.-J. Werner and P. J. Knowles with contributions from J. Almlöf, R. D. Amos, A. Berning, D. L. Cooper, M. J. O. Deegan, A. J. Dobbyn, F. Eckert, S. T. Elbert, C. Hampel, R. Lindh, A. W. Lloyd, W. Meyer, A. Nicklass, K. Peterson, R. Pitzer, A. J. Stone, P. R. Taylor, M. E. Mura, P. Pulay, M. Schütz, H. Stoll, and T. Thorsteinsson.

(10) Bergner, A.; Dolg, M.; Kuechle, W.; Stoll, H.; Preuss, H. *Mol. Phys.* **1993**, *80*, 1431; http://www.theochem.uni-stuttgart.de/pseudopotential/.

(11) Werner, H.-J.; Knowles, P. J. *J. Chem. Phys.* **1988**, *89*, 5803.

(12) Chau, F.-T.; Dyke, J. M.; Lee, E. P. F.; Wang, D.-C. *J. Electron. Spectrosc. Relat. Phenom.* **1998**, *97*, 33.

(13) Chen, P. Photoelectron Spectroscopy of Reactive Intermediates. In *Unimolecular and Bimolecular Reaction Dynamics*"; Ng, C. Y., et al., Eds.; John Wiley & Sons Ltd.: New York, 1994; pp 371−425.

(14) Leroy, R. J. *LEVEL 6.1: A Computer Program Solving the Radial Schrödinger equation for Bound and Quasibound levels, and Calculating Various Expectation Values and Matrix Elements*; University of Waterloo: Waterloo, Canada, 1996.

(15) Mok, D. K. W.; Lee, E. P. F.; Chau, F.-T.; Wang, D.-C.; Dyke, J. M. *J. Chem. Phys.* **2000**, *113*, 5791.

(16) Moore, C. E. *Atomic Energy Levels*; Natl. Bur. Stand., Circ. 467, U.S. Department of Commerce: Washington, DC, 1949.

(17) For examples: Haslett, T. L.; Fedrigo, S.; Bosnick, K.; Moskovits, M.; Duarte, H. A.; Salahub, D. *J. Am. Chem. Soc.* **2000**, *122*, 6039. Mortensen, J. J.; Hansen, L. B.; Hammer, B.; Norskov, J. K. *J. Catal.* **1999**, *182*, 479. Heinemann, C.; Schwarz, J.; Schwarz, H. *J. Phys. Chem.* **1996**, *100*, 6088. Ciullo, G.; Rosi, M.; Sgamelloti, A.; Floriani, C. *Chem. Phys. Lett.* **1991**, *185*, 522. Seigbahn, P. E. M.; Blomberg, M. R. A. *Chem. Phys.* **1984**, *87*, 189. Hidai, M.; Mizobe, Y. *Chem. Rev.* **1995**, *95*, 1115.

(18) Christe, K. O.; Wilson, W. W.; Sheehy, J. A.; Boatz, J. A. *Angew. Chem., Int. Ed. Engl.* **1999**, *38*, 2004.

(19) Chung, G.; Schmidt, M. W.; Gordon, M. S. *J. Phys. Chem. A* **2000**, *104*, 5647.

(20) Zheng, J. P.; Waluk, J.; Spanget-Larsen, J.; Blake, D. M.; Radziszewski, J. G. *Chem. Phys. Lett.* **2000**, *328*, 227.

(21) Manaa, M. R. *Chem. Phys. Lett.* **2000**, *331*, 262.

(22) Gagliardi, L.; Evangelisti, S.; Bernhardsson, A.; Lindh, R.; Roos, B. O. *Int. J. Quantum Chem.* **2000**, *77*, 311.

(23) Bittererova, M.; Brinck, T.; Ostmark, H. *J. Phys. Chem. A* **2000**, *104*, 11999.

(24) Li, Q. S.; Wang, L. J. *J. Phys. Chem. A* **2001**, *105*, 1203.

(25) Gagliardi, L.; Evangelisti, S.; Widmark, P.-O; Roos, B. O. *Theor. Chem. Acc.* **1997**, *97*, 136.